UC Davis

UC Davis Previously Published Works

Title

Diverse Synaptic Distributions of G Protein-coupled Estrogen Receptor 1 in Monkey Prefrontal Cortex with Aging and Menopause

Permalink

https://escholarship.org/uc/item/7sh2s928

Journal

Cerebral Cortex, 27(3)

ISSN

1047-3211

Authors

Crimins, Johanna L
Wang, Athena Ching-Jung
Yuk, Frank
et al.

Publication Date

2017-03-01

DOI

10.1093/cercor/bhw050

Peer reviewed

eScholarship.org Powered by the California Digital Library
University of California

Cerebral Cortex, March 2017;27:2022–2033

doi:10.1093/cercor/bhw050
Advance Access Publication Date: 3 March 2016
Original Article

ORIGINAL ARTICLE

Diverse Synaptic Distributions of G Protein-coupled Estrogen Receptor 1 in Monkey Prefrontal Cortex with Aging and Menopause

Johanna L. Crimins[1], Athena Ching-Jung Wang[6], Frank Yuk[1], Rishi Puri[1], William G. M. Janssen[1], Yuko Hara[1], Peter R. Rapp[7] and John H. Morrison[1,2,3,4,5]

[1]Fishberg Department of Neuroscience and Friedman Brain Institute, [2]Department of Geriatrics and Palliative Medicine, [3]Graduate School of Biomedical Sciences, Icahn School of Medicine at Mount Sinai, New York, NY 10029, USA, [4]California National Primate Research Center, Davis, CA 95616, USA, [5]Department of Neurology, School of Medicine, University of California Davis, Davis 95616, USA, [6]Linda Crnic Institute for Down Syndrome, University of Colorado School of Medicine, CO 80045, USA and [7]National Institute on Aging, Laboratory of Behavioral Neuroscience, Baltimore, MD 21224, USA

Address Correspondence to John H. Morrison, Ph.D., California National Primate Research Center, University of California Davis, One Shields Avenue, Davis, CA 95616, USA. Email: jhmorrison@ucdavis.edu

Abstract

Age- and menopause-related impairment in working memory mediated by the dorsolateral prefrontal cortex (dlPFC) occurs in humans and nonhuman primates. Long-term cyclic 17β-estradiol treatment rescues cognitive deficits in aged ovariectomized rhesus monkeys while restoring highly plastic synapses. Here we tested whether distributions of G protein-coupled estrogen receptor 1 (GPER1) within monkey layer III dlPFC synapses are sensitive to age and estradiol, and coupled to cognitive function. Ovariectomized young and aged monkeys administered vehicle or estradiol were first tested on a delayed response test of working memory. Then, quantitative serial section immunoelectron microscopy was used to determine the distributions of synaptic GPER1. GPER1-containing nonperforated axospinous synapse density was reduced with age, and partially restored with estrogen treatment. The majority of synapses expressed GPER1, which was predominately localized to presynaptic cytoplasm and mitochondria. GPER1 was also abundant at plasmalemmas, and within cytoplasmic and postsynaptic density (PSD) domains of dendritic spines. GPER1 levels did not differ with age or treatment, and none of the variables examined were tightly associated with cognitive function. However, greater representation of GPER1 subjacent to the PSD accompanied higher synapse density. These data suggest that GPER1 is positioned to support diverse functions key to synaptic plasticity in monkey dlPFC.

Key words: Area 46, delayed response, estradiol, GPER1, synapse

Introduction

In humans and nonhuman primates, the loss of circulating estrogen with menopause exacerbates normal age-related deficits in working memory, a higher-order cognitive function in which information is kept "in mind" in the absence of sensory stimulation to guide action, emotion, and thought (Bartus et al. 1978; Goldman-Rakic 1995; Roberts et al. 1997; Rapp et al. 2003; Arnsten et al. 2012; Hara, Rapp, et al. 2012; Hara et al. 2015; Lacreuse et al. 2015). Working memory is mediated by recurrent excitation of layer III pyramidal neuron circuits in the dorsolateral prefrontal cortex

© The Author 2016. Published by Oxford University Press. All rights reserved. For Permissions, please e-mail: journals.permissions@oup.com

(dlPFC) that are highly vulnerable to aging and menopause (Funahashi et al. 1989; Goldman-Rakic 1995; Hao et al. 2007; Dumitriu et al. 2010; Wang et al. 2011; Arnsten et al. 2012). In preclinical studies, we previously demonstrated that long-term cyclic administration of 17β-estradiol in aged ovariectomized rhesus monkeys reversed cognitive deficits measured by the well-characterized delayed response (DR) test of spatiotemporal working memory (Rapp et al. 2003; Hao et al. 2007). The age-related loss of highly plastic synapses observed on layer III dlPFC pyramidal neurons was also restored by estradiol treatment (Hao et al. 2007; Dumitriu et al. 2010). Recently, we reported that estrogen receptor ER-α, while likely important for working memory, was most abundant within synapses that remained stable with age, and regardless of circulating estrogen levels (Wang et al. 2010). Thus, whether the distributions of a specific estrogen receptor within dlPFC synapses are associated with the synaptic and procognitive effects of estradiol is yet to be determined.

G protein-coupled estrogen receptor 1 (GPER1) is expressed across multiple different regions along the rostrocaudal axis of the mammalian brain (Hazell et al. 2009; Naugle et al. 2014). It has been identified in rodent forebrain pyramidal neurons at extranuclear sites within the soma, and within both axonal and dendritic compartments (Almey et al. 2014; Waters et al. 2015). In synapses, GPER1 interacts with several structurally and functionally relevant proteins, such as spine scaffold protein PSD-95 and GluN2B-containing NMDA receptors, and may play a role in regulating spine density (Liu et al. 2012; Akama et al. 2013; Srivastava and Evans 2013; Gabor et al. 2015; Waters et al. 2015). Further, activation of GPER1 both modulates excitatory and inhibitory synaptic transmission, and improves learning and memory following ovariectomy in rodents (Hammond et al. 2009, 2012; Lebesgue et al. 2009, 2010; Liu et al. 2012, 2015; Hawley et al. 2014; Gabor et al. 2015).

A substantial literature now suggests that GPER1 exerts a wide range of neuroprotective actions, including a number targeting synaptic integrity (Lebesgue et al. 2009, 2010; Kosaka et al. 2012; Liu et al. 2012; Gaudet et al. 2015). For example, GPER1 agonist G1 reduced glutamate-induced excitotoxicity by attenuating NMDA receptor-elicited currents in cultured cortical neurons (Liu et al. 2012). In addition, GPER1 stimulation afforded protection from ischemic injury by activating a small-conductance calcium-activated potassium channel, and through modulation of excitatory synaptic responses in rodent hippocampal synapses (Lebesgue et al. 2009, 2010; Kosaka et al. 2012). Together, these findings raise the exciting possibility that estrogen may promote synaptic and cognitive health through GPER1-mediated signaling.

Using monkeys from our preclinical studies discussed above, the initial aim of the present investigation was to determine whether GPER1 was present in monkey dlPFC synapses and preferentially localized to distinct domains within a specific synaptic subclass; and, secondly to test for potential effects of age and estradiol on the distributions of synaptic GPER1 in relation to the integrity of prefrontal cortex-dependent working memory (Rapp et al. 2003; Hao et al. 2007; Wang et al. 2010). This research provides important clues as to how the anatomical positioning of GPER1 within monkey dlPFC synapses might support synaptic plasticity with age and menopause.

Materials and Methods

Animals

Thirteen young adult (mean ± SEM, 10.37 ± 0.65 years old) and 13 aged (mean ± SEM, 24.99 ± 0.70 years old) female rhesus monkeys (*Macaca mulatta*) were used in this study. These monkeys were part of a larger cohort used in a series of studies evaluating the effects of age and estradiol on cognition, and on several neurobiological parameters (Rapp et al. 2003; Hao et al. 2006, 2007; Yague et al. 2008; Wang et al. 2010). As such, all monkeys examined in the present study were previously behaviorally characterized, and the behavioral data for ovariectomized young and aged monkeys reported here were also included in Rapp et al. (2003) and Hao et al. (2007). Monkeys were singly housed in colonies of ~40 animals at the California National Primate Research Center, University of California, Davis. Water and monkey chow were provided in excess of nutritional needs. All experiments were conducted in compliance with the National Institutes of Health "Guidelines for the Care and Use of Experimental Animals," and were approved by the Institutional Animal Care and Use Committee at the University of California, Davis.

Monkeys as a Model for Aging and Menopause

Female rhesus monkeys are valuable models for studying aging, menopause, and related cognitive decline for several reasons. Like humans, rhesus monkeys are vulnerable to age- and menopause-related cognitive deficits. Importantly, their cognitive status can be quantified over the life course using a battery of cognitive tests that are similar to, if not the same as, those used in humans (Squire et al. 1988; Nagahara et al. 2010). Rhesus monkey neuroanatomy, neuronal gene expression, reproductive physiology, and patterns of endocrine senescence are all similar to those of women (Matt et al. 1998; Petrides and Pandya 1999; Gill et al. 2002; Woller et al. 2002; Nichols et al. 2005; Loerch et al. 2008; Walker and Herndon 2008; Hara, Rapp, et al. 2012). Notably, macaques undergo a low-estrogen menopause qualitatively similar to women, although relatively later in the lifespan (Gilardi et al. 1997; Nichols et al. 2005; Walker and Herndon 2008). Longevity in rhesus monkey is ~35 years, and the ratio with human aging has been estimated as 1:3 (Tigges et al. 1988). Finally, rhesus monkeys are not subject to Alzheimer's disease, so the effects of aging and menopause can be studied in the absence of neurodegenerative changes (Gearing et al. 1996; Sloane et al. 1997; Peters et al. 1999; Kimura et al. 2003),

DR Test

The DR test of spatiotemporal working memory was conducted as described previously (see Rapp et al. 2003 for details). Briefly, monkeys watched from behind a transparent screen while one of the lateral recessed wells of a test tray was baited with a food reward. Then, both lateral wells were covered with identical plaques, and an opaque screen was lowered to block the tray from view. Following a retention interval (i.e., a delay interval), the opaque screen was raised and monkeys were permitted to retrieve the food reward upon correct selection of the baited well. Left and right wells were baited equally across trials per testing session throughout the experiment. After animals initially learned procedural aspects of the DR task with short delays, memory was challenged with successively longer delay intervals of 5-, 10-, 15-, 30-, and 60-s (90 trials total/delay interval, 30 trials per day). Inter-trial interval was set to 20 s for the duration of testing.

Ovariectomy and 17β-estradiol Replacement

All monkeys included in this study received bilateral ovariectomies, and were randomly assigned to age-matched vehicle or estradiol treatment groups as part of earlier experiments

performed by our group (Rapp et al. 2003; Hao et al. 2007). Aged monkeys were premenopausal or perimenopausal at the time of surgery. Vehicle and estradiol treatments began following a post ovariectomy interval of 30 ± 1.7 weeks (mean ± SEM). Six of the animals available for this study per age group received 100 µg of estradiol cypionate (100 µg/ml sterile peanut oil, i.m.; Pharmacia) in a single injection every 21 days regardless of weight. The remaining 7 monkeys per age group included here received the same volume of vehicle according to the same administration schedule. Treatment extended over 2–3 years of behavioral testing, and animals were perfused 24 h following the final injection. Injection group designation and administration was coded, and all experimenters were blinded as per each of our studies involving the use of these monkeys (Rapp et al. 2003; Hao et al. 2006; 2007; Yague et al. 2008). Blind codes assigned at the beginning of this study were retained over its full course, including during all immunoelectron microscopy experiments and assessments, until statistical analyses were performed. Both serum 17β-estradiol and urine estrogen metabolite levels were measured at several time points, and ovariectomy reduced these levels to near zero (Shideler et al. 1993; Rapp et al. 2003). Following each injection, a rapid rise in circulating 17β-estradiol was observed in estradiol-, but not vehicle-treated monkeys. Estrogen levels peaked near values for ovary-intact female monkeys within 24 h of injection, after which they declined to baseline over the course of several days. Behavioral testing and endocrine treatments were continued to the time of perfusion.

Perfusion and Tissue Processing for Electron Microscopy

Twenty-four hours following the final injection of vehicle or estradiol, monkeys were sedated with ketamine hydrochloride (25 mg/kg), and deeply anesthetized with sodium pentobarbital (20–35 mg/kg, i.v.). They were then intubated and mechanically ventilated. Following a thoracotomy, 0.5% sodium nitrate (1.5 ml) was injected into the left ventricle of the heart, and the descending aorta was clamped. Monkeys were sacrificed by exsanguination while being perfused transcardially first with ice-cold 1% paraformaldehyde (PFA) in 0.1 M phosphate buffered saline (PBS; pH 7.2) for 1 min, and then with ice-cold 4% PFA in 0.1 M PBS for 12 min. Next, a craniotomy was performed, and the brain was removed and dissected in its entirety, including a frontal block containing the region surrounding the sulcus principalis (Brodmann's Area 46). The frontal block was postfixed in 4% PFA/0.125% glutaraldehyde in 0.1 M PBS for 6 h, and cut serially on a vibratome (Leica). Series of two 400-µm thick sections and ten 50-µm thick sections were collected across the entire rostrocaudal extent of Area 46; one 400-µm thick section per series was used for electron microscopy, and the other for experiments described in earlier work by our group (Hao et al. 2006, 2007). Freeze-substitution and low-temperature embedding of sections were performed as described previously (Adams et al. 2001, 2002; Yildirim et al. 2008). Briefly, sections were cryoprotected by immersion in increasing concentrations of glycerol in 0.1 M PB (10, 20, and 30% each for 2 h, then 30% overnight), and then rapidly plunged into liquid propane cooled by liquid nitrogen to −190°C in a Universal Cryofixation System KF80 (Reichert-Young). For en bloc fixation, cryoprotected sections were immersed in 1.5% uranyl acetate in anhydrous methanol (−90°C) for 24 h in a cryosubstitution Automatic Freeze-Substitution Stem unit (Leica). The temperature on the unit was then raised from −90 to −45°C in 4°C/h increments. The sections were washed with anhydrous methanol and infiltrated for 1 h each with progressively increasing concentrations of Lowicryl HM20 resin (Electron Microscopy Sciences) at −45°C followed by an overnight incubation with 100% Lowicryl. Ultraviolet light (360 nm) was used to polymerize the sections at −45°C for 48 h, and then at room temperature for 24 h. Five or more consecutive ultrathin (90-nm thick) sections each were cut on a Reichert-Jung ultramicrotome using a Diatome diamond knife (Electron Microscopy Sciences), and were mounted on an individual formvar-supported slot grid (Electron Micscopy Sciences) for subsequent immunoelectron microscopy experiments.

Postembedding Immunogold Labeling

A well-characterized rabbit polyclonal antibody raised against a synthetic peptide corresponding to the third extracellular domain of human GPER1 (amino acids 195–220), and purified by peptide immunogen affinity column, was obtained commercially (LS-A4271, MBL International Corporation) for use in this study. This antibody has been extensively tested, and previously shown by others to specifically recognize human GPER1 in a number of different tissues and cell types by Western blot analysis, and by immunohistochemistry (Isensee et al. 2009; Vivacqua et al. 2009; Lappano et al. 2010; Madeo and Maggiolini 2010; Madeo et al. 2010; Franco et al. 2011; Rago et al. 2011, 2014; Recchia et al. 2011). The specificity of the antibody was assessed in previous cell culture experiments using short hairpin RNA construct to knock down human GPER1 expression (Vivacqua et al. 2009; Lappano et al. 2010; Madeo and Maggiolini 2010; Madeo et al. 2010). The specificity of the antibody was further confirmed in the present study by performing a peptide adsorption control experiment with the immunizing peptide (LS-P4271; MBL International Corporation) in which no immunogold particle labeling was observed. Finally, electron microscopic immunocytochemistry showed that the antibody used here had comparable labeling patterns to another commercially available and well-characterized antibody (LS-A4272, MBL International Corporation) raised against human GPER1 (Akama et al. 2013; Waters et al. 2015).

Postembedding immunogold labeling was performed using methods similar to those described in our previous reports (Yildirim et al. 2008; Wang et al. 2010; Hara, Punsoni, et al. 2012; Bloss et al. 2013). Sections were first treated with 0.1% sodium borohydride/50 mM glycine in 0.3% NaCl/0.005 M Tris buffered saline (TBS) to remove excess aldehydes. They were then rinsed thoroughly with TBS, and incubated in TBS containing 2% human serum albumin (HSA) for 30 min at room temperature to block nonspecific binding of antisera. Next, sections were incubated in a rabbit polyclonal antibody raised against the third extracellular domain of human GPER1 (1:400 dilution; 2.5 µg/ml; MBL International Corporation) in 2% HSA/TBS overnight at room temperature. After thorough washing with TBS, sections were blocked with 2% HSA/TBS, and then incubated with the F(ab′) fragments of goat anti-rabbit IgG conjugated to 10 nm gold particles (1:40 dilution; Electron Microscopy Sciences), 2% HSA, and 5 mg/ml polyethylene glycol in TBS. Following a final thorough washing with TBS, sections were dried and then counterstained with 1% uranyl acetate for 45 min. The absence of gold particles when the primary antibody was omitted confirmed the specificity of the secondary antibody.

Quantitative Analysis of GPER1 Immunolabeling

All imaging and quantitative analyses of immunolabeling and synaptic morphology were performed by an experimenter who

was blind to both group designation and behavioral performance. Images were acquired at 80 kV with a Jeol 1200 EX transmission electron microscope equipped with an AMT Advantage CCD camera (Advanced Microscopy Techniques) using a systematic-random approach. Twenty image sets of 5 serial ultrathin sections for each monkey were captured at 6000× magnification in Area 46 layer III (~250–350 µm deep to the basal laminar aspect of layer I) of the dlPFC. As described in Hara, Punsoni et al. (2012), a principal goal of the present study was to provide a highly accurate and detailed characterization of synaptic immunolabeling patterns. For this reason, we chose to maximize the number of synapses included in analyses by using the third section as a reference section, and all synapses that possessed a dendritic spine with a clear postsynaptic density (PSD) visible in this section were marked and followed throughout the series for synapse immunolabeling and morphological assessments. More than 3200 total synapses, averaging > 100 synapses per monkey, were marked and analyzed. A synapse was classified as labeled if either the axon terminal or the dendritic spine contained one or more immunogold particles. This criterion was chosen given the high degree of specificity of the antibodies, and the near complete absence of gold particles observed in the peptide adsorption control experiment. For synapse areal density, the combined number of synapses marked in each reference section was expressed as a function of the sum total image area. Using criteria similar to those employed extensively by our group (He et al. 2000; Wang et al. 2010; Hara, Punsoni, et al. 2012; Bloss et al. 2013), 4 presynaptic bins, and 4 postsynaptic bins were used to categorize the location of each gold particle within a labeled synapse. The presynaptic bins were: (1) the active zone (within 30 nm of the presynaptic membrane, and directly apposed to a spine PSD that was visible in the reference section); (2) the plasmalemmal bin (within 30 nm of the plasma membrane, but outside the presynaptic active zone); (3) the cytoplasmic bin (the axon terminal core >30 nm from the plasma membrane, and outside the active zone); and, (4) the mitochondrial bin (within 30 nm of the mitochondrial outer membrane, the mitochondrial core, and on sections adjacent to those containing the last visible mitochondrion). The postsynaptic bins were: (1) the synaptic bin, which included the synaptic cleft, the PSD (within 30 nm of the postsynaptic membrane), and the perisynaptic zone (the plasma membrane located within 30 nm of the lateral edges of the PSD, and on sections adjacent to those containing the last visible PSD); (2) the subsynaptic bin (subjacent to the synaptic zone, but within 60 nm of the postsynaptic membrane); (3) the plasmalemmal bin (within 30 nm of the plasma membrane, but outside the synaptic bin); and, (4) the cytoplasmic bin (the core of the dendritic spine >30 nm from the plasma membrane, and outside the synaptic and subsynaptic bins).

Morphological data were obtained for each labeled and unlabeled synapse using measurement tools available in Adobe Photoshop CS5 Extended (version 12.0.4 ×64, Adobe systems Incorporated). The diameter of each presynaptic terminal was determined using the ruler tool to measure the maximal width oriented parallel to the presynaptic active zone. The lasso tool was used to measure the area of each presynaptic mitochondrion across the 5 serial sections. The head diameter and PSD lengths (across the 5 serial sections) for each dendritic spine were measured using the ruler tool. For perforated synapses, which were defined by the presence of a discontinuous PSD visible in any of the 5 serial sections, the length of each PSD segment was measured individually. For each synapse, the total PSD length (combined lengths of all PSD segments across the 5 serial sections) was multiplied by the section thickness (90 nm) to derive the PSD area; this was also used as an area estimate for the synaptic cleft, the subsynaptic bin, and the presynaptic active zone. For the perisynaptic area, the combined lengths of the perisynaptic zones across the 5 serial sections were added to twice the smallest PSD length, which was then multiplied by the section thickness. Similar to our previous work (Hara, Punsoni, et al. 2012), cytoplasmic volume and plasmalemmal surface area estimates were derived for each axon terminal and spine using the measured diameter as the diameter value for a sphere, and for a half of a sphere, respectively. Each electron micrograph was adjusted in its entirety for brightness, contrast, and sharpness using Adobe Photoshop CS5 Extended (version 12.0.4 ×64, Adobe systems Incorporated).

Methodological Considerations

Serial section immunoelectron microscopy is the best available method for high-resolution, detailed assessment of the ultrastructural and molecular organization of individual synapses. We have previously established that a series of 5 ultrathin sections is ideal for highly accurate assessments of synapse morphology (Hara, Punsoni, et al. 2012; Bloss et al. 2013). While most postsynaptic densities were reliably captured in their entirety within each series, this was not always the case. However, the proportion of synapses categorized as such did not differ between groups (multivariate ANOVA and one-way ANOVA; P values > 0.05; data not shown). Finally, as with previous work by our group, the present study was designed to obtain the maximal amount of information for each synapse across a large population, with a principal focus on the comprehensive quantitative assessment of immunogold labeling (Hara, Punsoni, et al. 2012; Bloss et al. 2013). To this end, we chose a synapse sampling scheme that we believe effectively harnessed the advantages of serial compared with single section methods. While we cannot rule out that this procedure was subject to bias, we expect that such bias would be far less than a single section analysis and largely equivalent across all groups. Importantly, the determination of the number of synaptic profiles per unit micrograph area (synapse areal density) allowed for assessment of the relative changes in synapse density between groups, despite that estimates of absolute values would likely differ from those reported here. Synapse density data in this study closely correlated with our previous estimates in individual layer III dlPFC neurons from the same monkeys (Pearson's correlation; $n = 22$ monkeys, $r = 0.425$, $P = 0.049$), confirming that the subset of synapses selected for inclusion accurately represented the population as a whole (Hao et al. 2007).

Statistical Analyses

All statistical analyses were performed using IBM SPSS Statistics software version 20 (IBM Corporation). All behavioral and neurobiological data followed a normal distribution (one-sample Kolmogorov–Smirnov test, P values >0.05), and accordingly, parametric statistics were applied. A repeated-measures ANOVA was used to determine whether DR performance accuracy at successively longer delay intervals differed across age and/or treatment groups. A multivariate ANOVA with age and treatment as fixed factors was used to compare all neurobiological measures. A one-way multivariate ANOVA was then used to assess possible differences in these measures across the 4 groups (young OVX + V, young OVX + E, aged OVX + V, aged OVX + E). Tukey's *post hoc* tests were performed to assess between-group differences while correcting for multiple comparisons. To verify that a

sufficient sample size was used to support the data, observed power was determined using an ANOVA. A Student's *t* test (equal variance not assumed) was used to compare means where indicated. A bivariate Pearson's product–moment correlation was used to determine relationships between variables. Because of the limited number of monkeys available for analysis, together with the risk of overcorrection, Pearson product–moment correlations were not corrected for multiple comparisons. All analyses were 2-tailed, and significance was defined as $P \leq 0.05$ for all statistical tests. All data are reported as the mean ± SEM, calculated based on one aggregate (i.e., average) value per animal.

Results

Modest Improvement in DR Performance in Aged Ovariectomized Monkeys with Estrogen Replacement

The subset of 26 monkeys included in the present study was part of a larger cohort examined in earlier work by our group (Rapp et al. 2003; Hao et al. 2006, 2007; Yague et al. 2008; Wang et al. 2010). Therefore, DR data for monkeys in this study were also included in Rapp et al. (2003) and Hao et al. (2007), and our behavioral findings are described in detail in these manuscripts. DR accuracy across increasing memory delays (5-, 10-, 15-, 30-, and 60 -s) for the subset of monkeys available for inclusion here is shown in Figure 1. Percent correct scores declined significantly across delays of 5- to 60-s (repeated-measures ANOVA; main delay effect, $F_{1,22} = 17.045$, $P < 0.0001$, observed power = 1.000), confirming that the test effectively interrogated working memory. Group difference failed to reach significance (repeated-measures ANOVA; main group effect; $P = 0.100$), likely in large part due to high within-group variance in this subset of monkeys that is smaller than in the original report; high variance was especially evident in the young group in which a number of monkeys exhibited unexpectedly poor performance (Rapp et al. 2003; Hao et al. 2007). However, in agreement with Rapp et al. (2003), performance accuracy was notably numerically lower in aged ovariectomized (OVX) monkeys administered vehicle (V) versus estradiol (E). As published previously, aged OVX + E monkeys performed at a level that was nearly equivalent to that of young OVX and ovary-intact monkeys (Rapp et al. 2003; Hao et al. 2007). Finally, DR task performance was insensitive to ovarian hormone status in young OVX monkeys, consistent with findings from other groups (Voytko 2000). Thus, young monkeys may have greater cognitive resiliency (high DR performance accuracy), regardless of the presence of circulating estrogens (Hao et al. 2007).

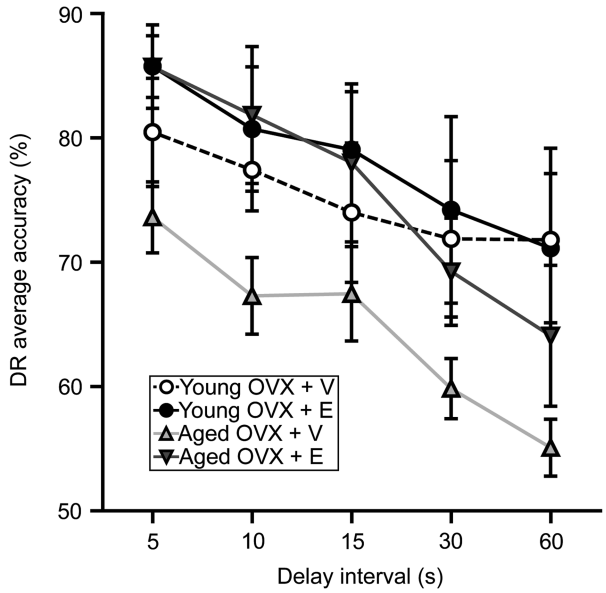

Figure 1. DR task performance accuracy. V, vehicle; E, estradiol. Group results are expressed as the mean ± SEM. Young OXV + V, $n = 7$; young OVX + E, $n = 6$; aged OVX + V, $n = 7$; aged OVX + E, $n = 6$.

Partial Restoration of GPER1-containing Synapses with Estrogen Replacement in Aged Ovariectomized Monkeys

We previously reported a significant age-related decrease in the density of spines along dendrites of individual Lucifer yellow-filled layer III PFC pyramidal neurons from OVX monkeys (Hao et al. 2007). In the present study, assessment at the ultrastructural level in a subset of these same monkeys revealed a qualitatively similar reduction in the areal density of synapses in aged compared with young OVX monkeys (multivariate ANOVA; main age effect, $F_{1,22} = 14.777$, $P = 0.001$, observed power = 0.957; Figure 2*A*). This age-dependent loss of synapses persisted when analyses were restricted to synapses containing GPER1 immunogold particles (main age effect, $F_{1,22} = 13.971$, $P = 0.001$, observed power = 0.946; Figure 2*B*), then when analyses were further restricted to GPER1-containing synapses with nonperforated (main age effect, $F_{1,22} = 7.08$, $P = 0.014$, observed power = 0.720; Figure 2*C*), but not with perforated ($P > 0.05$; Fig. 2*D*) postsynaptic densities (PSDs). Despite the lack of a significant interaction between age and treatment factors ($P > 0.05$), synapses—specifically GPER1-containing synapses with nonperforated PSDs—were numerically partially rescued in aged OVX monkeys with estrogen replacement. Notably, the heads of nonperforated synapse spines included in this ultrastructural dataset were on average similar in diameter (~ 0.4 μm) to the small, highly plastic spines that we had previously shown to be particularly vulnerable to aging and estrogen deprivation (Hao et al. 2007). Thus, the estradiol-dependent partial restoration of these smaller, nonperforated synapse spines in aged OVX monkeys observed here compliment this previous report demonstrating at the ultrastructural level that these synapses contain GPER1 (Hao et al. 2007).

A one-way ANOVA across all 4 groups (young OVX + V, young OVX + E, aged OVX + V, aged OVX + E) was performed in order to determine whether neurobiological measures were statistically different between select groups. This analysis revealed a significant main effect of group for the areal densities of synapses (one-way ANOVA; $F_{3,22} = 6.01$, $P = 0.004$, observed power = 0.918), GPER1-containing synapses ($F_{3,22} = 5.071$, $P = 0.005$, observed power = 0.902), and GPER1-containing synapses with nonperforated PSDs ($F_{3,22} = 3.541$, $P = 0.031$, observed power = 0.705). Tukey's post hoc comparisons showed that the areal density of synapses in aged OVX + V monkeys was significantly lower than in both young OVX + V ($P = 0.007$) and young OVX + E ($P = 0.010$) monkeys, while the latter groups did not differ from one another ($P > 0.05$; Fig. 2*A*). Areal density of synapses in aged OVX + V monkeys also did not significantly differ from those of aged OVX + E monkeys ($P > 0.05$). This pattern persisted when analyses were restricted to GPER1-containing synapses (aged OVX + V vs. young OVX + V, $P = 0.01$; aged OVX + V vs. young OVX + E, $P = 0.011$; young OXV + V vs. young OVX + E, $P > 0.05$; aged OVX + V vs. aged OVX + E, $P > 0.05$; Fig. 2*B*); and, when only GPER1-containing synapses with nonperforated PSDs were considered (aged OVX + V vs. young OVX + V, $P = 0.047$; aged OVX + V vs. young OVX + E, $P = 0.004$; young OXV + V vs. young OVX + E, $P > 0.05$; aged OVX + V

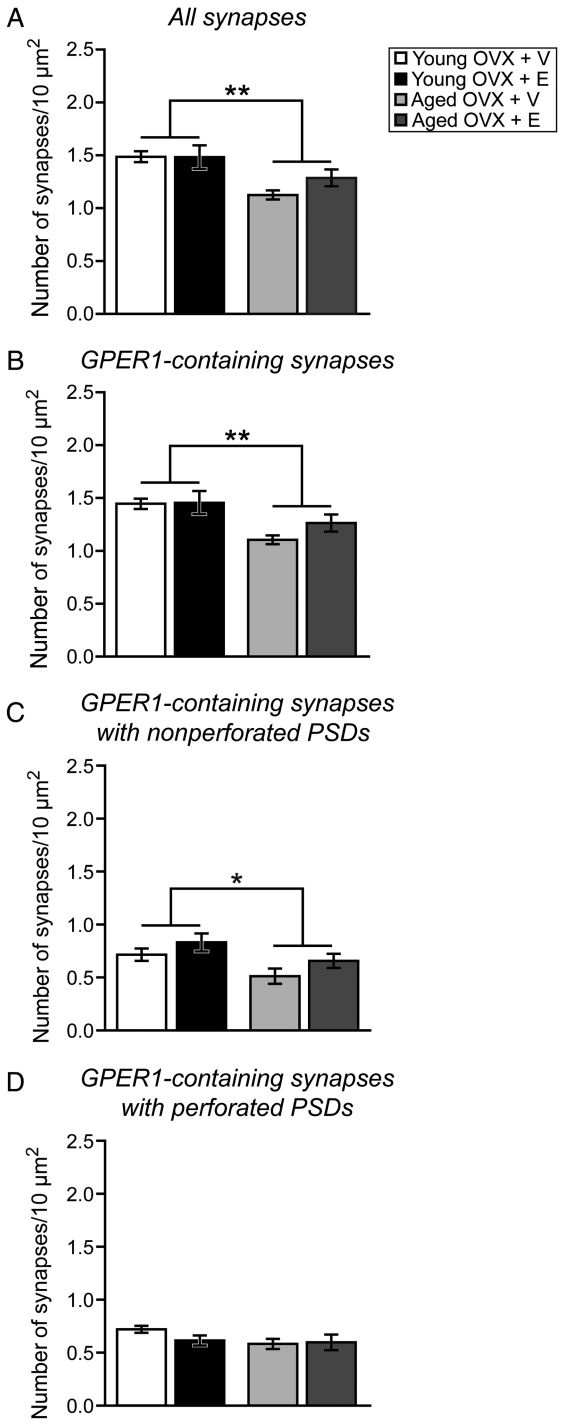

Figure 2. Age effects on areal densities of synapses. (*A*), Areal density of the total population of synapses. (*B*), Areal density of synapses that contained GPER1 immunogold particles. (*C*), Areal density of GPER1-containing synapses that possessed nonperforated postsynaptic densities. (*D*), Areal density of GPER1-containing synapses that possessed perforated postsynaptic densities. V, vehicle; E, estradiol. Group results are expressed as the mean ± SEM. Significant age effects indicated by $^{*}P < 0.05$ and $^{**}P < 0.01$. Young OXV + V, $n = 7$; young OVX + E, $n = 6$; aged OVX + V, $n = 7$; aged OVX + E, $n = 6$.

vs. aged OVX + E, $P > 0.05$; Fig. 2*C*). Unlike aged OVX + V monkeys, aged OVX + E monkeys exhibited areal density measures similar to, albeit numerically lower than young OVX monkeys in both treatment groups, regardless of GPER1 content, or PSD type (P values > 0.05).

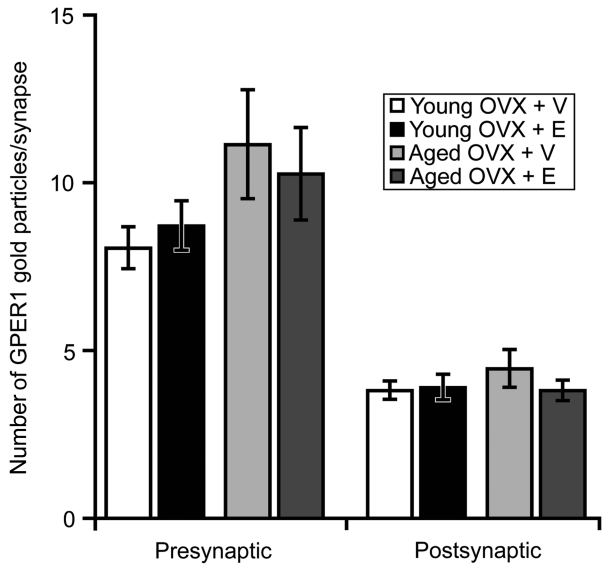

Figure 3. Densities of GPER1 immunogold particles in the presynaptic and postsynaptic compartments. V, vehicle; E, estradiol. Group results are expressed as the mean ± SEM. Young OXV + V, $n = 7$; young OVX + E, $n = 6$; aged OVX + V, $n = 7$; aged OVX + E, $n = 6$.

Abundance and Subcellular Distributions of GPER1-containing Synapses Across Age and Hormone Status

The majority of axon terminals (93%) and dendritic spines (81%) assessed contained GPER1 immunogold particles. Thus, most synapses contained GPER1 immunogold particles within either the presynaptic, or the postsynaptic compartment (i.e., within the axon terminal or the dendritic spine, respectively), and were classified as labeled. The percentage of synapses containing GPER1 did not differ with age or treatment status (multivariate ANOVA), and was similar across all 4 groups of monkeys (one-way ANOVA; P values >0.05; data not shown). The average number of GPER1 gold particles in axon terminals and dendritic spines also failed to differ with age or treatment status (multivariate ANOVA), or between groups (one-way ANOVA; P values >0.05; Fig. 3) indicating that GPER1 expression levels remain relatively stable with age and estrogen status. Further, the number of gold particles localized to the presynaptic compartment was approximately 2-fold that of the postsynaptic compartment for each of 4 groups (Fig. 3), a finding that likely reflects the significantly larger size of axon terminals relative to dendritic spines (mean ± SEM; diameter, axon terminal = 0.838 ± 0.017 µm vs. dendritic spine = 0.550 ± 0.006 µm; Student's t-test, $t_{25} = -17.814$, $P = 0.0001$).

To determine whether the subcellular distributions of GPER1 were different with age or hormone status, each gold particle was classified as belonging to 1 of 8 synaptic bins (4 pre- and 4 postsynaptic bins) based on its location within an individual synapse followed across 5 serial ultrathin sections (Fig. 4*A*,*B*). There were no significant effects of age or treatment status (multivariate ANOVA), or reliable between-group effects (one-way ANOVA) on the number of GPER1 gold particles within any of the 8 synaptic bins (P values >0.05; data not shown). These synaptic binning distributions did, however, demonstrate that GPER1 was predominately localized to the cytoplasm (often associated with synaptic vesicles) and mitochondria of axon terminals, comprising 33% and 24% of the sum total number of gold particles per synapse, respectively (Fig. 4*C*). GPER1 was also highly enriched in the plasmalemmal domains of both terminals and spines, as well

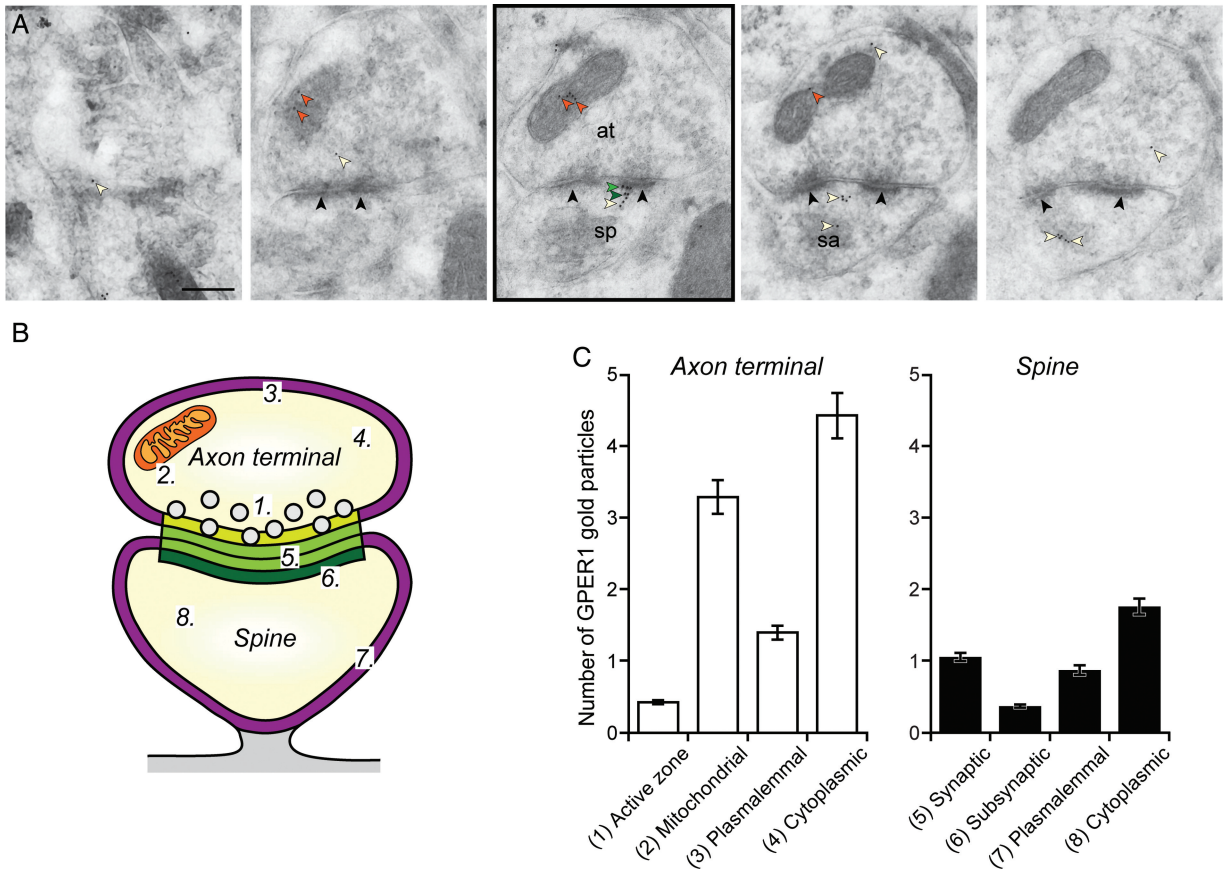

Figure 4. Subcellular synaptic distribution of GPER1 immunogold particles. (*A*), Representative electron micrographs of 5 serial sections through a GPER1-containing perforated synapse spine. The postsynaptic density is readily apparent (black arrowheads). GPER1 immunogold particles are shown localized to mitochondrial (orange arrowheads), cytoplasmic (light beige arrowheads), synaptic (light green arrowheads), and subsynaptic (dark green arrowheads) domains. For each series, the third section (outlined with a black box) was used as a reference section, and all synapses that possessed a dendritic spine with a clear postsynaptic density in this section were marked and followed throughout the series for morphological and immunolabeling assessments. At, axon terminal; sp, dendritic spine; sa, spine apparatus. Scale bar, 250 nm. (*B*), Schematic diagram illustrating the 8 synaptic domains used to categorize the location of each GPER1 immunogold particle: active zone (1); mitochondrial (2); plasmalemmal, axon terminal (3); cytoplasmic, axon terminal (4); synaptic (5); subsynaptic (6); plasmalemmal, spine (7); and, cytoplasmic, spine (8). (*C*), Plots of the number of GPER1 immunogold particles within axon terminal (left), and dendritic spine (right) compartments averaged across all monkeys. Data are expressed as the mean ± SEM. $n = 3141$ synapses.

as in the cytoplasmic and synaptic (comprised of both the PSD and bordering perisynaptic region) domains of spines. Within the spine cytoplasm, GPER1 was often present on endomembranous structures, including the spine apparatus (Fig. 4A). The localization of GPER1 to the PSD and presynaptic active zone is qualitatively similar to patterns previously observed by others in rodent hippocampal and prefrontal cortical synapses (Akama et al. 2013; Waters et al. 2015).

To test for potential shifts in synaptic dimensions that might accompany the overall stability observed in GPER1 immunogold particle number, the densities of GPER1 immunogold particles were calculated for each synaptic domain (see Materials & Methods for details). There were no significant effects of age or treatment status (multivariate ANOVA), or between-group effects (one-way ANOVA) on the density of GPER1 gold particles in any of the 8 synaptic domains (*P* values >0.05).

Lower Percentage of GPER1 Within the Subsynaptic Domain of Synapses From Aged Ovariectomized Monkeys and its Association with Synapse Density

To assess possible age- or treatment-dependent shifts in the distributions of GPER1 immunogold particles across synaptic domains, the number of gold particles localized to each synaptic bin was expressed as a percentage of the total number of gold particles in either the presynaptic or the postsynaptic compartment. A multivariate ANOVA showed a main effect of age ($F_{1,22} = 8.218$, $P = 0.009$, observed power = 0.782), but not of treatment ($P > 0.05$), on the percentage of postsynaptic GPER1 immunogold particles localized specifically within the subsynaptic domain (Fig. 5A). Overall, the percentage of postsynaptic GPER1 within this domain was ~23% lower in spines from aged compared with young OVX monkeys, regardless of the presence of circulating estrogens. Tukey's post hoc comparisons showed a significantly lower percentage of postsynaptic gold particles in the subsynaptic domain of spines from aged OVX + E versus young OVX + E ($P = 0.048$). There was no effect of age or treatment (multivariate ANOVA), or of group (one-way ANOVA) on the percentage of immunogold particles localized to any other pre- or postsynaptic domain (*P* values >0.05; data not shown).

Bivariate Pearson's correlation analyses were used to evaluate potential relationships between GPER1 distributions and synapse density. A positive relationship emerged between the percentage of postsynaptic GPER1 in the subsynaptic domain and the areal density of GPER1-containing synapses (Pearson's correlation; $n = 26$ monkeys, $r = 0.432$, $P = 0.028$; Fig. 5B, left). When analyses

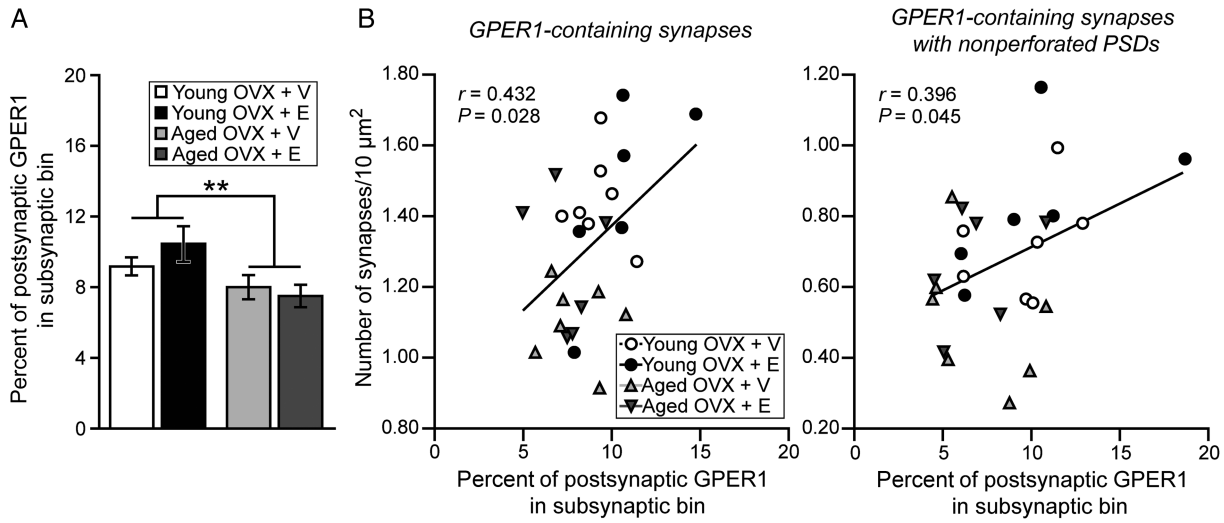

Figure 5. Percentage of postsynaptic GPER1 immunogold particles localized to the subsynaptic domain, and its relationship to synapse areal density. (*A*), Bar graph of the percentage of postsynaptic GPER1 immunogold particles localized to the subsynaptic domain of GPER1-containing synapses. (*B*), Positive correlation between the percentage of postsynaptic GPER1 immunogold particles localized to the subsynaptic domain and the areal density of GPER1-containing synapses (left), and of GPER1-containing synapses with nonperforated PSDs (right) for each monkey. V, vehicle; E, estradiol. Group results are expressed as the mean ± SEM. Significant age effect indicated by $^{**}P < 0.01$. Young OXV + V, $n = 7$; young OVX + E, $n = 6$; aged OVX + V, $n = 7$; aged OVX + E, $n = 6$.

were restricted to GPER1-containing synapses with nonperforated PSDs, the association between postsynaptic GPER1 in the subsynaptic domain and synapse density persisted (Pearson's correlation; $n = 26$ monkeys, $r = 0.396$, $P = 0.045$; Fig. 5*B*, right). The relationship between subsynaptic GPER1 and synapse density was altogether absent for perforated synapse spines (Pearson's correlation; $n = 26$ monkeys, $r = 0.152$, $P > 0.05$; data not shown).

No Correlation Between Synaptic Distributions of GPER1 and Individual DR Accuracy

GPER1 is a membrane receptor that interacts with PSD proteins, and may influence second messenger systems that impact synaptic plasticity and cognition. Therefore, bivariate Pearson's correlation analyses were used to test whether synaptic GPER1, and GPER1 localized within other postsynaptic compartments, was associated with working memory performance (average DR accuracy); these correlations, however, did not reach the significance level.

Discussion

This study is the first investigation of the precise subcellular distributions of GPER1 within synapses of monkey dlPFC, and their potential regulation with aging and surgical menopause. GPER1 was localized to the majority of synapses, including a small, nonperforated spine synapse subclass lost with age, and partly restored with cyclic estrogen treatment. It was widely distributed across multiple synaptic domains, and its expression was largely stable with age and ovarian hormone status. Greater representation of subsynaptic GPER1 was associated with higher synapse density, but there was no apparent correlation between synaptic GPER1 distributions and working memory performance on an individual subject basis. An integrative model of the proposed relationship of synaptic GPER1 distributions with aging and estradiol is shown in Figure 6. Together, our results suggest that GPER1 is strategically positioned to modulate synaptic plasticity, and that its synaptic localization is coupled to synapse density.

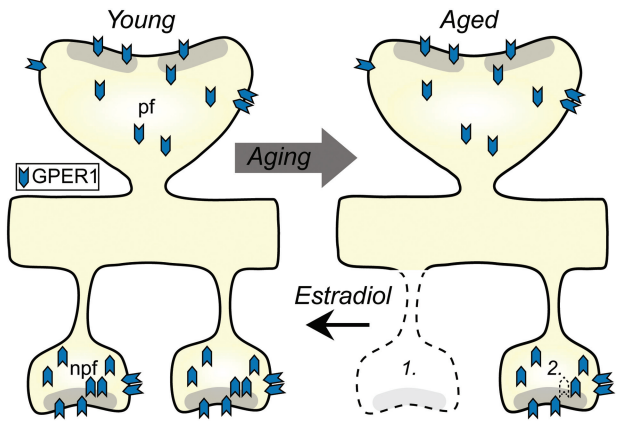

Figure 6. Schematic diagram illustrating proposed relationships of GPER1 distributions to aging and estradiol treatment. Nonperforated synapse spines containing GPER1 are lost with age, but are partially restored to levels of young monkeys with estrogen treatment (1). The percentage of GPER1 immunogold particles localized to the subsynaptic domain of nonperforated, but not of perforated, synapse spines is lower in aged than in young monkeys, and is associated with a low synapse density (2). Diagrams were drawn based on current results as well as data from previous work (Hao et al. 2006, 2007). Npf, nonperforated; pf, perforated.

Age and Estradiol Effects on the Areal Density of Synapses Containing GPER1

We previously determined by single section immunoelectron microscopy that approximately half of dlPFC synapses from the same monkeys examined here were labeled for ER-α (Wang et al. 2010). However, because the 2-dimensional approach used in our earlier work tends to underestimate the number of labeled profiles, it is possible that the percentage of ER-α-containing synapses was, in actuality, somewhat higher (Yildirim et al.

2008; Bloss et al. 2013). That a markedly high percentage of monkey dlPFC synapses contained GPER1 relative to ER-α is in agreement with findings from a recent study by Almey et al. (2014) indicating that GPER1 is twice as abundant as estrogen receptor ER-α in female rat medial PFC. It is important to note that the primary antibody chosen to detect GPER1 in the present study was well characterized, and extensively tested (Isensee et al. 2009; Vivacqua et al. 2009; Lappano et al. 2010; Madeo and Maggiolini 2010; Madeo et al. 2010; Franco et al. 2011; Rago et al. 2011; Recchia et al. 2011; Almey et al. 2014). Antibody specificity was confirmed in cell culture experiments using short hairpin RNA construct to knock down human GPER1 expression (Vivacqua et al. 2009; Lappano et al. 2010; Madeo and Maggiolini 2010; Madeo et al. 2010) and, in our hands, by a peptide adsorption control experiment demonstrating the absence of immunogold labeling. The areal density of GPER1-containing synapses was significantly lower with age, primarily due to the specific loss of synapses that possessed nonperforated, but not perforated, postsynaptic densities (PSDs). This finding compliments our previous confocal microscopy report of spine loss with age and estrogen deprivation in individual dlPFC neurons from the same monkeys (Hao et al. 2007). The average head diameter of nonperforated synapse spines included here was similar to that of the small, thin spines described at the confocal level, which likely possessed nonperforated PSDs almost exclusively (Bourne and Harris 2007; Hao et al. 2007). This highly plastic morphological subclass is considered a critical synaptic substrate for dlPFC-dependent cognitive tasks such as the DR task, and is an important index of plasticity in the aging brain (Kasai et al. 2003, 2010; Holtmaat et al. 2005; Hao et al. 2007; Dumitriu et al. 2010; Morrison and Baxter 2014). Whether GPER1 function specifically targets the health of small synapses remains to be determined. However, there is evidence that GPER1 mediates excitatory synaptic transmission through selective regulation of GluN2B-containing NMDA receptors that typically dominate this synapse type (Liu et al. 2012; Liu and Zhao 2013). How our data support a possible role for GPER1 in promoting nonperforated synapse spine density is discussed in detail below.

Subcellular Sites of GPER1 and its Regulation with Age and Estradiol

The localization of GPER1 to dendritic spines, and to axon terminals where it was markedly abundant, is consistent with studies in rodent forebrain (Akama et al. 2013; Almey et al. 2014; Waters et al. 2015). Within these compartments, GPER1 was distributed to the plasmalemmal and cytoplasmic domains; to the postsynaptic density and its subjacent subsynaptic zone; and, to the active zone and presynaptic mitochondria. Many cytoplasmic GPER1 gold particles were associated with membranous structures, such as synaptic vesicles in the axon terminals and the spine apparatus postsynaptically. Such highly diversified subcellular localizations suggest that GPER1 mediates the complex activities of estrogen within the synapse, as well as other spine and terminal domains.

We found that GPER1 distributions were largely insensitive to age and to circulating estrogen levels. These results extend our previous finding that ER-α levels were also stable within dlPFC synapses from the same monkeys (Wang et al. 2010). Our data showing insensitivity of GPER1 abundance to estrogen treatment is consistent with a recent study in mice showing that GPER1 distributions in hippocampal synapses between males and females, and across estrous cycle stage, were comparable (Waters et al. 2015). However, they found that high levels of estrogen (proestrus phase) were associated with increased axonal GPER1 expression in females. Thus, age and/or estrogen-dependent changes in GPER1 expression may be specific to select species, brain regions, or neuronal compartments.

Relationship Between Subsynaptic GPER1 Expression and Synapse Areal Density

The percentage of GPER1 immunogold particles localized to the subsynaptic domain was significantly decreased with age. Low subsynaptic GPER1 representation was associated with low synapse densities, and this was often the case for aged monkeys regardless of hormone status. Conversely, young monkeys generally exhibited high GPER1 representation in this domain, together with high synapse densities. These relationships were driven predominately by small nonperforated synapse spines as the correlation failed to reach significance when analyses were restricted to the perforated subclass.

The association between subsynaptic GPER1 and spine density is consistent with recent findings that GPER1-expressing cortical neurons had a significantly higher spine density versus control neurons, and that GPER1 agonist G1 rapidly increased dendritic spine density in OVX mouse hippocampus (Srivastava and Evans 2013; Gabor et al. 2015). Generally, estrogen-induced increases in spine density have been attributed to activation of intracellular signaling cascades important for actin remodeling, which is highly dynamic in smaller synapses, whereas actin polymerization during remodeling processes can enhance spine stability (Fischer et al. 1998; Hering and Sheng 2001). Within the subsynaptic zone, GPER1 is ideally positioned to link synaptic receptor activity to such signaling cascades, including the MAPK/ERK pathway (Harris and Kater 1994; Fischer et al. 1998; Sanchez et al. 2012; Srivastava et al. 2013; Sellers et al. 2015). We previously demonstrated at the ultrastructural level that phosphorylated-LIM kinase (p-LIMK), which critically regulates actin dynamics through phosphorylation of cofilin, is highly enriched in the synaptic and subsynaptic domains of rat hippocampal and PFC synapses (Yildirim et al. 2008; Bloss et al. 2013). It has been postulated that GPER1 activation initiates early upstream events in the LIMK-cofilin cascade, however this possibility has yet to be explored empirically (Waters et al. 2015). Interactions between GPER1 and spine scaffolding proteins such as PSD-95 and SAP97 may also be key to understanding the linkage between subsynaptic GPER1 and synaptic density (Akama et al. 2013; Waters et al. 2015). Future studies are needed to more finely resolve the precise mechanisms underlying this important relationship, and their downstream effects on the functional capacities of dlPFC.

Absence of Association Between Synaptic GPER1 Distributions and Working Memory Performance

The present study failed to demonstrate a significant, within-subject relationship between subcellular distributions of GPER1 in dlPFC synapses and individual performance accuracy on the DR test of working memory. Therefore, while our results are consistent with the possibility that changes in synaptic GPER1 are among the cascade of events that contribute to compromised memory-related synaptic plasticity in the aged primate dlPFC, these changes may not be the proximal cause of working memory impairment in a tight one-to-one association. This finding is an important one in view of the growing body of evidence from rodent studies supporting the beneficial effects of GPER1 activation on learning and memory processes (Hammond et al. 2009, 2012; Hawley et al. 2014; Gabor et al. 2015). The behavioral

consequences of GPER1 may be species-, or task-dependent, or reliant on its precise neuronal distributions and actions within specific brain regions. In addition, receptor function, rather than number, may be a major factor. For example, the ability of GPER1 to trigger cell signaling cascades may be altered with aging and/or estrogen deprivation. It is also possible that coordinate physiological responses of a precise complement of estrogen receptors in monkey dlPFC synapses, rather than of any given receptor alone, ultimately contributes to estrogen-sensitive cognitive processes.

Conclusion

A detailed understanding of the molecular profiles of optimally healthy synapses is a prerequisite for identifying potential approaches for promoting successful cognitive aging. In the present study, we demonstrated that GPER1 is ideally positioned to support diverse functions important to the modulation of synaptic plasticity in monkey dlPFC with aging and menopause for the first time. One principal outcome from this work was the possibility that estrogenic action on synapse density may be mediated, in part, by GPER1 within the dendritic spine subsynaptic domain. Hence, the precise distributions of GPER1 within the synapse may have important implications for synaptic health, and may represent a future therapeutic target.

Funding

This work was supported by National Institutes of Health grants R37 AG06647 and P01 AG16765 to J.H.M., and in part by the Intramural Research Program of the National Institute on Aging.

Notes

We thank Anne Canfield, Sania Fong, Deborah Kent, Heather McKay, Tweithy Oung, and Mary Roberts at the California National Primate Research Center for their expert technical assistance involving the rhesus monkeys, and Dr Donald Canfield for assistance in veterinary work. We also thank Katina Calakos for assistance with data acquisition. *Conflict of Interest:* None declared.

References

Adams MM, Fink SE, Shah RA, Janssen WG, Hayashi S, Milner TA, McEwen BS, Morrison JH. 2002. Estrogen and aging affect the subcellular distribution of estrogen receptor-alpha in the hippocampus of female rats. J Neurosci. 22:3608–3614.

Adams MM, Shah RA, Janssen WG, Morrison JH. 2001. Different modes of hippocampal plasticity in response to estrogen in young and aged female rats. Proc Natl Acad Sci U S A. 98:8071–8076.

Akama KT, Thompson LI, Milner TA, McEwen BS. 2013. Post-synaptic density-95 (PSD-95) binding capacity of G-protein-coupled receptor 30 (GPR30), an estrogen receptor that can be identified in hippocampal dendritic spines. J Biol Chem. 288:6438–6450.

Almey A, Cannell E, Bertram K, Filardo E, Milner TA, Brake WG. 2014. Medial prefrontal cortical estradiol rapidly alters memory system bias in female rats: ultrastructural analysis reveals membrane-associated estrogen receptors as potential mediators. Endocrinology. 155:4422–4432.

Arnsten AF, Wang MJ, Paspalas CD. 2012. Neuromodulation of thought: flexibilities and vulnerabilities in prefrontal cortical network synapses. Neuron. 76:223–239.

Bartus RT, Fleming D, Johnson HR. 1978. Aging in the rhesus monkey: debilitating effects on short-term memory. J Gerontol. 33:858–871.

Bloss EB, Puri R, Yuk F, Punsoni M, Hara Y, Janssen WG, McEwen BS, Morrison JH. 2013. Morphological and molecular changes in aging rat prelimbic prefrontal cortical synapses. Neurobiol Aging. 34:200–210.

Bourne J, Harris KM. 2007. Do thin spines learn to be mushroom spines that remember? Curr Opin Neurobiol 17:381–386.

Dumitriu D, Hao J, Hara Y, Kaufmann J, Janssen WG, Lou W, Rapp PR, Morrison JH. 2010. Selective changes in thin spine density and morphology in monkey prefrontal cortex correlate with aging-related cognitive impairment. J Neurosci. 30:7507–7515.

Fischer M, Kaech S, Knutti D, Matus A. 1998. Rapid actin-based plasticity in dendritic spines. Neuron. 20:847–854.

Franco R, Boscia F, Gigantino V, Marra L, Esposito F, Ferrara D, Pariante P, Botti G, Caraglia M, Minucci S, et al. 2011. GPR30 is overexpressed in post-puberal testicular germ cell tumors. Cancer Biol Ther. 11:609–613.

Funahashi S, Bruce CJ, Goldman-Rakic PS. 1989. Mnemonic coding of visual space in the monkey's dorsolateral prefrontal cortex. J Neurophysiol. 61:331–349.

Gabor C, Lymer J, Phan A, Choleris E. 2015. Rapid effects of the G-protein coupled oestrogen receptor (GPER) on learning and dorsal hippocampus dendritic spines in female mice. Physiol Behav. 149:53–60.

Gaudet HM, Cheng SB, Christensen EM, Filardo EJ. 2015. The G-protein coupled estrogen receptor, GPER: The inside and inside-out story. Mol Cell Endocrinol. 418 Pt 3:207–219.

Gearing M, Tigges J, Mori H, Mirra SS. 1996. A beta40 is a major form of beta-amyloid in nonhuman primates. Neurobiol Aging. 17:903–908.

Gilardi KV, Shideler SE, Valverde CR, Roberts JA, Lasley BL. 1997. Characterization of the onset of menopause in the rhesus macaque. Biol Reprod. 57:335–340.

Gill S, Sharpless JL, Rado K, Hall JE. 2002. Evidence that GnRH decreases with gonadal steroid feedback but increases with age in postmenopausal women. J Clin Endocrinol Metab. 87:2290–2296.

Goldman-Rakic PS. 1995. Cellular basis of working memory. Neuron. 14:477–485.

Hammond R, Mauk R, Ninaci D, Nelson D, Gibbs RB. 2009. Chronic treatment with estrogen receptor agonists restores acquisition of a spatial learning task in young ovariectomized rats. Horm Behav. 56:309–314.

Hammond R, Nelson D, Kline E, Gibbs RB. 2012. Chronic treatment with a GPR30 antagonist impairs acquisition of a spatial learning task in young female rats. Horm Behav. 62:367–374.

Hao J, Rapp PR, Janssen WG, Lou W, Lasley BL, Hof PR, Morrison JH. 2007. Interactive effects of age and estrogen on cognition and pyramidal neurons in monkey prefrontal cortex. Proc Natl Acad Sci U S A. 104:11465–11470.

Hao J, Rapp PR, Leffler AE, Leffler SR, Janssen WG, Lou W, McKay H, Roberts JA, Wearne SL, Hof PR, et al. 2006. Estrogen alters spine number and morphology in prefrontal cortex of aged female rhesus monkeys. J Neurosci. 26:2571–2578.

Hara Y, Punsoni M, Yuk F, Park CS, Janssen WG, Rapp PR, Morrison JH. 2012. Synaptic distributions of GluA2 and PKMzeta in the monkey dentate gyrus and their relationships with aging and memory. J Neurosci. 32:7336–7344.

Hara Y, Rapp PR, Morrison JH. 2012. Neuronal and morphological bases of cognitive decline in aged rhesus monkeys. Age (Dordr). 34:1051–1073.

Hara Y, Waters EM, McEwen BS, Morrison JH. 2015. Estrogen effects on cognitive and synaptic health over the lifecourse. Physiol Rev. 95:785–807.

Harris KM, Kater SB. 1994. Dendritic spines: cellular specializations imparting both stability and flexibility to synaptic function. Annu Rev Neurosci. 17:341–371.

Hawley WR, Grissom EM, Moody NM, Dohanich GP, Vasudevan N. 2014. Activation of G-protein-coupled receptor 30 is sufficient to enhance spatial recognition memory in ovariectomized rats. Behav Brain Res. 262:68–73.

Hazell GG, Yao ST, Roper JA, Prossnitz ER, O'Carroll AM, Lolait SJ. 2009. Localisation of GPR30, a novel G protein-coupled oestrogen receptor, suggests multiple functions in rodent brain and peripheral tissues. J Endocrinol. 202:223–236.

He Y, Janssen WG, Rothstein JD, Morrison JH. 2000. Differential synaptic localization of the glutamate transporter EAAC1 and glutamate receptor subunit GluR2 in the rat hippocampus. J Comp Neurol. 418:255–269.

Hering H, Sheng M. 2001. Dendritic spines: structure, dynamics and regulation. Nat Rev Neurosci. 2:880–888.

Holtmaat AJ, Trachtenberg JT, Wilbrecht L, Shepherd GM, Zhang X, Knott GW, Svoboda K. 2005. Transient and persistent dendritic spines in the neocortex in vivo. Neuron. 45:279–291.

Isensee J, Meoli L, Zazzu V, Nabzdyk C, Witt H, Soewarto D, Effertz K, Fuchs H, Gailus-Durner V, Busch D, et al. 2009. Expression pattern of G protein-coupled receptor 30 in LacZ reporter mice. Endocrinology. 150:1722–1730.

Kasai H, Fukuda M, Watanabe S, Hayashi-Takagi A, Noguchi J. 2010. Structural dynamics of dendritic spines in memory and cognition. Trends Neurosci. 33:121–129.

Kasai H, Matsuzaki M, Noguchi J, Yasumatsu N, Nakahara H. 2003. Structure-stability-function relationships of dendritic spines. Trends Neurosci. 26:360–368.

Kimura N, Tanemura K, Nakamura S, Takashima A, Ono F, Sakakibara I, Ishii Y, Kyuwa S, Yoshikawa Y. 2003. Age-related changes of Alzheimer's disease-associated proteins in cynomolgus monkey brains. Biochem Biophys Res Commun. 310:303–311.

Kosaka Y, Quillinan N, Bond C, Traystman R, Hurn P, Herson P. 2012. GPER1/GPR30 activation improves neuronal survival following global cerebral ischemia induced by cardiac arrest in mice. Transl Stroke Res. 3:500–507.

Lacreuse A, Mong JA, Hara Y. 2015. Neurocognitive effects of estrogens across the adult lifespan in nonhuman primates: State of knowledge and new perspectives. Horm Behav. 74:157–166.

Lappano R, Rosano C, De Marco P, De Francesco EM, Pezzi V, Maggiolini M. 2010. Estriol acts as a GPR30 antagonist in estrogen receptor-negative breast cancer cells. Mol Cell Endocrinol. 320:162–170.

Lebesgue D, Chevaleyre V, Zukin RS, Etgen AM. 2009. Estradiol rescues neurons from global ischemia-induced cell death: multiple cellular pathways of neuroprotection. Steroids. 74:555–561.

Lebesgue D, Traub M, De Butte-Smith M, Chen C, Zukin RS, Kelly MJ, Etgen AM. 2010. Acute administration of non-classical estrogen receptor agonists attenuates ischemia-induced hippocampal neuron loss in middle-aged female rats. PLoS One. 5:e8642.

Liu SB, Tian Z, Guo YY, Zhang N, Feng B, Zhao MG. 2015. Activation of GPR30 attenuates chronic pain-related anxiety in ovariectomized mice. Psychoneuroendocrinology. 53:94–107.

Liu SB, Zhang N, Guo YY, Zhao R, Shi TY, Feng SF, Wang SQ, Yang Q, Li XQ, Wu YM,, et al. 2012. G-protein-coupled receptor 30 mediates rapid neuroprotective effects of estrogen via depression of NR2B-containing NMDA receptors. J Neurosci. 32:4887–4900.

Liu SB, Zhao MG. 2013. Neuroprotective effect of estrogen: role of nonsynaptic NR2B-containing NMDA receptors. Brain Res Bull. 93:27–31.

Loerch PM, Lu T, Dakin KA, Vann JM, Isaacs A, Geula C, Wang J, Pan Y, Gabuzda DH, Li C,, et al. 2008. Evolution of the aging brain transcriptome and synaptic regulation. PLoS One. 3: e3329.

Madeo A, Maggiolini M. 2010. Nuclear alternate estrogen receptor GPR30 mediates 17beta-estradiol-induced gene expression and migration in breast cancer-associated fibroblasts. Cancer Res. 70:6036–6046.

Madeo A, Vinciguerra M, Lappano R, Galgani M, Gasperi-Campani A, Maggiolini M, Musti AM. 2010. c-Jun activation is required for 4-hydroxytamoxifen-induced cell death in breast cancer cells. Oncogene. 29:978–991.

Matt DW, Kauma SW, Pincus SM, Veldhuis JD, Evans WS. 1998. Characteristics of luteinizing hormone secretion in younger versus older premenopausal women. Am J Obstet Gynecol. 178:504–510.

Morrison JH, Baxter MG. 2014. Synaptic health. JAMA Psychiatry. 71:835–837.

Nagahara AH, Bernot T, Tuszynski MH. 2010. Age-related cognitive deficits in rhesus monkeys mirror human deficits on an automated test battery. Neurobiol Aging. 31:1020–1031.

Naugle MM, Nguyen LT, Merceron TK, Filardo E, Janssen WG, Morrison JH, Rapp PR, Gore AC. 2014. G-protein coupled estrogen receptor, estrogen receptor alpha, and progesterone receptor immunohistochemistry in the hypothalamus of aging female rhesus macaques given long-term estradiol treatment. J Exp Zool A Ecol Genet Physiol. 321:399–414.

Nichols SM, Bavister BD, Brenner CA, Didier PJ, Harrison RM, Kubisch HM. 2005. Ovarian senescence in the rhesus monkey (*Macaca mulatta*). Hum Reprod. 20:79–83.

Peters A, Jones EG, Morrison JH. 1999. Cerebral cortex: neurodegenerative and age-related changes in structure and function of cerbral cortex. New York: Springer.

Petrides M, Pandya DN. 1999. Dorsolateral prefrontal cortex: comparative cytoarchitectonic analysis in the human and the macaque brain and corticocortical connection patterns. Eur J Neurosci. 11:1011–1036.

Rago V, Giordano F, Brunelli E, Zito D, Aquila S, Carpino A. 2014. Identification of G protein-coupled estrogen receptor in human and pig spermatozoa. J Anat. 224:732–736.

Rago V, Romeo F, Giordano F, Maggiolini M, Carpino A. 2011. Identification of the estrogen receptor GPER in neoplastic and non-neoplastic human testes. Reprod Biol Endocrinol. 9:135.

Rapp PR, Morrison JH, Roberts JA. 2003. Cyclic estrogen replacement improves cognitive function in aged ovariectomized rhesus monkeys. J Neurosci. 23:5708–5714.

Recchia AG, De Francesco EM, Vivacqua A, Sisci D, Panno ML, Ando S, Maggiolini M. 2011. The G protein-coupled receptor 30 is up-regulated by hypoxia-inducible factor-1alpha (HIF-1alpha) in breast cancer cells and cardiomyocytes. J Biol Chem. 286:10773–10782.

Roberts JA, Gilardi KV, Lasley B, Rapp PR. 1997. Reproductive senescence predicts cognitive decline in aged female monkeys. Neuroreport. 8:2047–2051.

Sanchez AM, Flamini MI, Polak K, Palla G, Spina S, Mannella P, Genazzani AD, Simoncini T. 2012. Actin cytoskeleton remodelling by sex steroids in neurones. J Neuroendocrinol. 24:195–201.

Sellers K, Raval P, Srivastava DP. 2015. Molecular signature of rapid estrogen regulation of synaptic connectivity and cognition. Front Neuroendocrinol. 36:72–89.

Shideler SE, Ortuno AM, Moran FM, Moorman EA, Lasley BL. 1993. Simple extraction and enzyme immunoassays for estrogen and progesterone metabolites in the feces of *Macaca fascicularis* during non-conceptive and conceptive ovarian cycles. Biol Reprod. 48:1290–1298.

Sloane JA, Pietropaolo MF, Rosene DL, Moss MB, Peters A, Kemper T, Abraham CR. 1997. Lack of correlation between plaque burden and cognition in the aged monkey. Acta Neuropathol. 94:471–478.

Squire LR, Zola-Morgan S, Chen KS. 1988. Human amnesia and animal models of amnesia: performance of amnesic patients on tests designed for the monkey. Behav Neurosci. 102: 210–221.

Srivastava DP, Evans PD. 2013. G-protein oestrogen receptor 1: trials and tribulations of a membrane oestrogen receptor. J Neuroendocrinol. 25:1219–1230.

Srivastava DP, Woolfrey KM, Penzes P. 2013. Insights into rapid modulation of neuroplasticity by brain estrogens. Pharmacol Rev. 65:1318–1350.

Tigges J, Gordon TP, McClure HM, Hall EC, Peters A. 1988. Survival rate and life span of rhesus monkeys at the Yerkes regional primate research Center. Am J Primatol. 15:263–273.

Vivacqua A, Lappano R, De Marco P, Sisci D, Aquila S, De Amicis F, Fuqua SA, Ando S, Maggiolini M. 2009. G protein-coupled receptor 30 expression is up-regulated by EGF and TGF alpha in estrogen receptor alpha-positive cancer cells. Mol Endocrinol. 23:1815–1826.

Voytko ML. 2000. The effects of long-term ovariectomy and estrogen replacement therapy on learning and memory in monkeys (*Macaca fascicularis*). Behav Neurosci. 114:1078–1087.

Walker ML, Herndon JG. 2008. Menopause in nonhuman primates? Biol Reprod. 79:398–406.

Wang AC, Hara Y, Janssen WG, Rapp PR, Morrison JH. 2010. Synaptic estrogen receptor-alpha levels in prefrontal cortex in female rhesus monkeys and their correlation with cognitive performance. J Neurosci. 30:12770–12776.

Wang M, Gamo NJ, Yang Y, Jin LE, Wang XJ, Laubach M, Mazer JA, Lee D, Arnsten AF. 2011. Neuronal basis of age-related working memory decline. Nature. 476:210–213.

Waters EM, Thompson LI, Patel P, Gonzales AD, Ye HZ, Filardo EJ, Clegg DJ, Gorecka J, Akama KT, McEwen BS, et al. 2015. G-protein-coupled estrogen receptor 1 is anatomically positioned to modulate synaptic plasticity in the mouse hippocampus. J Neurosci. 35:2384–2397.

Woller MJ, Everson-Binotto G, Nichols E, Acheson A, Keen KL, Bowers CY, Terasawa E. 2002. Aging-related changes in release of growth hormone and luteinizing hormone in female rhesus monkeys. J Clin Endocrinol Metab. 87:5160–5167.

Yague JG, Wang AC, Janssen WG, Hof PR, Garcia-Segura LM, Azcoitia I, Morrison JH. 2008. Aromatase distribution in the monkey temporal neocortex and hippocampus. Brain Res. 1209:115–127.

Yildirim M, Janssen WG, Tabori NE, Adams MM, Yuen GS, Akama KT, McEwen BS, Milner TA, Morrison JH. 2008. Estrogen and aging affect synaptic distribution of phosphorylated LIM kinase (pLIMK) in CA1 region of female rat hippocampus. Neuroscience. 152:360–370.